Available online at www.CivileJournal.org

Civil Engineering Journal

(E-ISSN: 2476-3055; ISSN: 2676-6957)

Vol. 10, No. 01, January, 2024

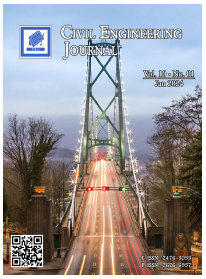

Flexural Behavior of Repaired Reinforced Concrete Beams Due to Corrosion of Steel Reinforcement Using Grouting and FRP Sheet Strengthening

Rudy Djamaluddin [1*], Rita Irmawaty [1], Fakhruddin [1], Kohei Yamaguchi [2]

[1] *Department of Civil Engineering, Faculty of Engineering, Hasanuddin University, South Sulawesi 91711, Indonesia.*

[2] *Department of Civil Engineering, Nagasaki University, Nagasaki, Japan.*

Received 11 September 2023; Revised 24 November 2023; Accepted 15 December 2023; Published 01 January 2024

Abstract

One of the common causes of damage to the concrete structures close to the sea line is corrosion on the steel reinforcement in the concrete, which may cause spalling on the concrete cover. This paper presents the results of the simulation of the corroded reinforced concrete beams, which were repaired using the grouting method and FRP strengthening. The concrete cover of the beam specimens on the tensile side was filled with grouted concrete instead of filled with normal concrete to simulate the repair of concrete spalling. Three types of beam specimens were prepared and tested under a monotonic loading. BG and BPF were the specimens for beams with grouting only and beams with grouting and flexural strengthening using FRP sheets, respectively. Flexural strengthening using FRP sheets was carried out to restore the flexural capacity. As a comparison, control beams were also prepared in the form of normal reinforced concrete (BN). The results showed that the BG beam had a capacity of only about 50% compared to the control beam (BN). However, applying flexural strengthening using FRP sheet as on the type BGF beams showed that it had approximately the same capacity as BN specimens. This indicated that the repair method using grouting on damaged concrete covers and strengthening using FRP sheets was an effective alternative to repairing the corroded reinforced concrete beams.

Keywords: Steel Reinforced Concrete; Repairing; Corrosion; Grouting; FRP.

1. Introduction

The development progress of a country is mainly determined by the development of its infrastructure. One type of construction that is widely used in infrastructure development is reinforced concrete (RC) structures because it has economic advantages and durability. However, the massive development of infrastructure, especially RC structures, has the potential to cause environmental impacts if the infrastructure has to be demolished. Concrete materials generally produce highly alkaline leachates [1]. In some developed countries, such as America, it was estimated that 15 to 30% of solid waste disposed of in landfills was construction waste; even in European countries, more than half of solid waste was construction waste [1–3]. Figure 1 shows the demolition waste of RC structures that have no longer been able to continue their service lives. To minimize the impact on the environment, the service life of the structure needs to be optimized, for example, by strengthening weakened structures or repairing damaged structures, either due to disasters or aggressive environmental attack.

* Corresponding author: rudydj@unhas.ac.id; rudy0011@gmail.com

http://dx.doi.org/10.28991/CEJ-2024-010-01-014

Figure 1. Solid waste from construction demolishing

Reinforced concrete structures in coastal areas have a very high risk of damage due to the aggressive marine environment. Although concrete is a relatively durable construction material, it is not enough to guarantee the durability of the construction as a system if the steel reinforcement as a structural component experiences corrosion. The marine environment, which contains elements of salt, can seep through the pores of the concrete and penetrate the concrete reinforcement [4]. As a result, the steel reinforcement in the concrete may experience corrosion and loss due to the infiltration of chloride ions in the seawater environment. The chloride ion is corrosive and can attack the calcium silicate binding system [5–7]. Figure 2 shows a photo of a steel-reinforced concrete beam experiencing corrosion on the reinforcement. The corroded reinforcement may expand and cause longitudinal cracks and spalling in the reinforced concrete cover, which results in a decrease in the strength and service life of the structures. Beams that have been corroded on the steel reinforcement due to the influence of chloride attacks from the marine environment or due to the carbonation process will expand and cause longitudinal cracks around the concrete cover, resulting in spalling, as illustrated in Figure 3. This causes a decrease in the nominal moment capacity of reinforced concrete beams [8–11].

(a) Longitudinal crack (b) Corrosion of steel rebars

Figure 2. Deterioration of Reinforced Concrete beams due to corrosion of steel rebars

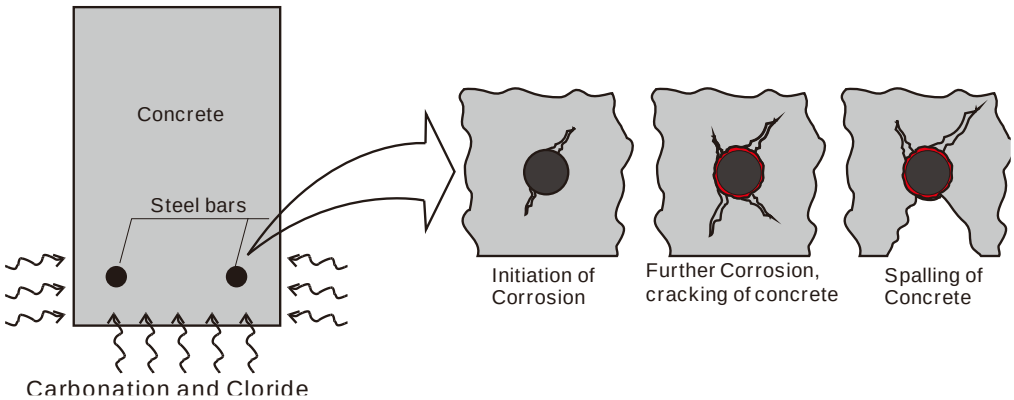

Figure 3. Corrosion propagation due to Carbonation and Chloride attack

In some construction projects in coastal areas, it is difficult to avoid the corrosion of steel reinforcement. However, with consideration of the environmental impact and the high cost of new construction, structures that have been corroded should not always end in demolition. The deteriorated structures should be considered to be repaired to extend the service life of the structure. Alternative solutions are needed to minimize construction waste by developing a repair concept for existing structures that have experienced premature deterioration so that demolition can be avoided. Grouting concrete material is a material that is often used for repairs to concrete structures, such as crack repairs and porous concrete repairs.

Repairing or strengthening the reinforced concrete beams has been proposed by some researchers to extend the service life of the structures. Wrapping grout with metallic connectors was developed to increase the flexural capacity of concrete beams [12–15]. A repair alternative to rehabilitate corrosion-defected reinforced concrete (RC) beam-column members has been developed using new mortar on damaged concrete covers [8]. The jacketing method in repairing the damaged RC beams resulted in an increase in the flexural strength of the repaired beams [16]. A research focus on repairing spalled reinforced concrete structures using a polymer-modified cementitious mortar has also been developed [17]. Patching using grouting has also been applied to repair corrosion-defected reinforced concrete beam-column members [10]. Following the introduction of advanced materials, several strengthening techniques have been developed, in particular by utilizing advanced fiber-reinforced plastic (FRP) materials [18–20]. Masoud & Soudki [19] conducted an experimental study on the corrosion activity of reinforced concrete beams repaired with fiber-reinforced polymer (FRP) sheets. The corroded beams were repaired with FRP sheets. Results indicated that mass loss of the main reinforcing bars due to corrosion was reduced by up to 16% because of the effect of the existing FRP sheet as a protector as well as the strengthening materials. The field of structure repair is growing with the presence of advanced FRP materials. The use of FRP, often also referred to as a composite material, is an advanced material that is currently increasingly popular for use in various applications, especially in the field of construction improvement [20–23].

FRP has the advantage of being a material that is more resistant to extreme environmental conditions and has good mechanical properties [24–26]. Research related to repair techniques using FRP materials is growing more widely. Figure 4 shows a photo example of repairs with grouting and structural repairs using FRP sheet material. Research in the repair of corroded concrete structures has been studied. Most research was conducted on repairing with grouting mortar or strengthening with FRP separately. Canaval et al. [13] have conducted an investigation on reinforced concrete beams strengthened by wrapping grouting mortar with metallic connectors. Alwash et al. [15] studied the efficiency of patch repair to rehabilitate corrosion-defected reinforced concrete (RC) beam-column members when exposed to bending moments and axial forces. He concluded that the corroded reinforced concrete beams showed a significant deterioration in their structural performance and integrity. This may reduce the ultimate capacity, stiffness, serviceability, and ductility of the beams. The results indicated that the flexural capacity of the strengthened beams increased by about 44%, and the failure was due to shear. Do-Dai et al. applied CFRP laminate to strengthen corroded concrete beams [27]. The research focuses on the repair of corroded reinforced concrete beam structures using grouting concrete combined with FRP strengthening. Research in this field has not been carried out comprehensively. There are still very limited discussions about the repair of corroded concrete beams in combination with grouting and FRP strengthening. This paper introduces an alternative method for repairing corroded reinforced concrete beam structures using grouting concrete combined with FRP strengthening.

(a) Repairing using concrete grouting (b) Strengthening using CFRP Sheet

Figure 4. Repairing and Strengthening of Reinforced concrete beams

The concept of this method is that the spalling or cracking concrete cover is repaired by the grouting method, whereas the reduced moment capacity due to mass loss of the steel reinforcement area is recovered using external strengthening with FRP sheet material attached to the outer side of the tensile section (outer surface of grouting). It is noted here that the shear forces that arise at the joints (cold joints) between the existing concrete and the grouted concrete are an important factor in ensuring good integrity (full-bonded). The integrity of the bonding surface has an influence on the bending mechanism's ability to produce optimal flexural capacity. In order to ensure the bonding capacity, it was done by using an adhesive (bonding agent) on the cold joint, followed by surface roughening to produce a wider bonding area. Figure 5 presents a flow chart to briefly show the process of the repair methodology.

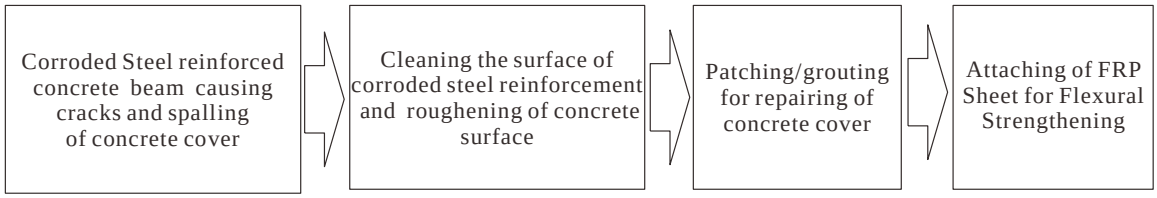

Figure 5. Process of the Repairing methodology

2. Experimental Program

2.1. Specimens

The dimensions of reinforced concrete beams for laboratory testing were 150 × 200 mm with a length (L) of 3300 mm. Two types of beam specimens were prepared, which are BG and BGF. The BG was a repaired beam without FRP reinforcement (only grouting concrete), and the BGF was a repaired beam with FRP sheet strengthening, respectively. In addition, BN specimens were also prepared as a control beam. Table 1 shows the variations of the specimens, and Figure 6 shows the details of the beam specimens. The specimens for control beams (BN) were designed to use 3D13 mm (three bars of 13 mm diameter) as tensile reinforcement with a concrete strength of f'c = 25 MPa. The control beams were designed to have a theoretical moment capacity of 15 kNm. For beam specimens of BG and BGF, steel reinforcements of 3D10 were used as tensile reinforcement with the same arrangement and configuration as the BN beams. A smaller diameter of tensile reinforcement on BG and BGF was used to simulate a mass loss due to the corrosion of tensile reinforcement. In this case, it was assumed that the initial cross-section of steel reinforcement with a diameter of 13 mm (D13) decreased to 10 mm (D10), or 40% of its original cross-section. Details of the specimens are shown in Figure 6.

Table 1. Type of specimens

No.	Type of Specimen	Specimen Name	Number of Specimen	Purposes
1	BN	Control Specimen	3	Control specimens
2	BG	Beam with grouting	3	Investigate the effectiveness of repairing using only grouting.
3	BGF	Beam with grouting and FPR strengthening	3	Investigate the effectiveness of repairing using grouting and strengthened by FRP sheet

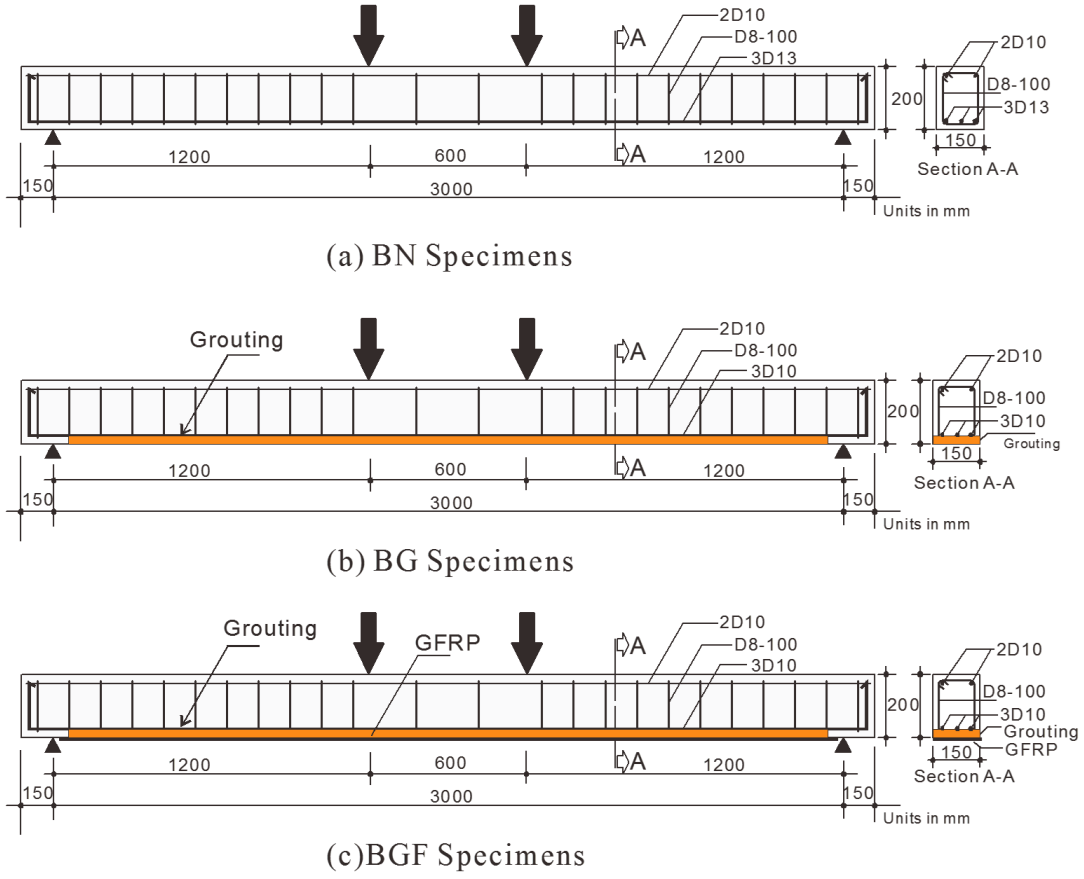

Figure 6. Detail of Specimens

Prior to casting, several strain gauges were installed on the steel reinforcement to measure the strain. The casting of concrete was carried out in the opposite direction, where the bottom of the beams was on the upper side, for convenience in grouting the concrete cover. BN specimens were cast as on the regular reinforced concrete beam. On repaired beams (BG and BGF), the casting process was divided into two steps. Firstly, the normal concrete material was casted up to the tension reinforcement level (as a simulation of the concrete cover spalling), and it was cured in wet conditions for two weeks at room temperature and humidity conditions. When the first step of concrete casting had hardened, the second step was conducted by casting grouting concrete as thick as the concrete cover (a simulation of repairing the spalled concrete cover). Prior to grouting, the concrete surface was cleaned with a wire brush. A bonding agent was used to increase the bonding interaction between normal concrete and grouted concrete. The grouting process was carried out on the entire length of the beam. The grouted concrete was cured for 7 days to harden the grout. Figure 7 shows the sequences of the grouting process for beam specimens.

Figure 7. Grouting Process of the Beams

Only the beam specimen of BGF (repair and strengthening) was attached to the FRP sheet according to the attachment standards recommended by the manufacturer. Glass fiber-reinforced polymer sheet (GFRP sheet) was used for flexural strengthening of beams. The specimens were cured for 3 days until the FRP adhesive had hardened and bonded perfectly with the concrete surface. Table 2 shows the properties of the materials used in this study.

Table 2. Mechanical Properties of Materials

Material Name	Tensile Strength (MPa)	Compressive Strength (MPa)	Modulus of Elasticity (GPa)
Normal Concrete	-	23.51	-
Grout Concrete	-	31.75	-
Steel bar D10	417	-	200
Steel bar D13	430	-	200
GFRP*	983	-	57

* Based on data sheet of manufacturer.

2.2. Test Setup

Figure 8 shows the test setup for beam specimens. The specimens were loaded under flexural loading with a four-point loading system monotonically using static test equipment with a capacity of 150 tons. Prior to testing, the horizontal and vertical lines with a spacing of 50 mm were drawn at one side of the beam specimens for cracking observation.

Figure 8. Test Setup

Strain gauges were attached on the outer side of the compression section (upper side of the beam) and also on the side of the beam section to measure the strain that occurs during the loading process. The strain gauges on the sides of beams were attached to evaluate the distribution of strain that occurs on the compressive section of the beam. The beam specimens were placed on the support as a simple beam. The Linear Variable Displacement Transducer (LVDT) deflection gauge with an accuracy of 0.01 mm was placed under the beam at the mid-span point and at the point of loading. The load was applied gradually under displacement control at a rate of 0.2 mm/sec. The applied load was monitored through a load cell with a capacity of 200 kN and an accuracy of 0.1 kN. All the instruments were connected to a data logger. A computer connected to a data logger was used to show the measured value at each load step. During the loading simulation process, observations were made on the increase in load and strain that occurred, including the deflection of the beam. During the loading, the appearance of cracks was observed as well as the failure mode.

3. Results and Discussions

3.1. Flexural Capacity

Table 3 shows a summary of the flexural capacity of the specimens. For the control beam (BN), the average load causing initial cracking occurred when the load reached 4.15 kN, or M_{cr} equal to 3.28 kNm. The tensile reinforcement reached the yield stress when the load reached 25.93 kN, or M_y equal to 16.35 kNm. The ultimate beam capacity was achieved when the load reached 28.98 kN, or M_u equal to 18.18 kNm. It should be noted here that the estimated moment capacity of the test beam ($M_{u\text{-}est}$) was 15.00 kN. The ultimate moment capacity M_u of the beam was relatively higher than the estimated ultimate moment ($M_{u\text{-}est}$) with a ratio of 1.26.

Table 3. Summary of Flexural Capacity of Specimens

Specimen Name	P_u(kN)	M_u(kN.m)	P_y(kN)	M_y(kN.m)	P_u(kN)	M_u(kN.m)	Mu_{est}(kN.m)	M_u/Mu_{est}
BN#1	5.21	3.92	26.51	16.70	27.86	17.51	15.00	1.17
BN#2	5.38	4.02	27.63	17.37	28.44	17.86	15.00	1.19
BN#3	1.86	1.91	23.66	14.99	30.64	19.18	15.00	1.28
Average	4.15	3.28	25.93	16.35	28.98	18.18	15.00	1.21
BG#1	3.46	2.87	11.98	7.98	14.72	9.63	11.56	0.83
BG#2	1.08	1.44	12.61	8.36	14.38	9.42	11.56	0.83
BG#3	2.61	2.36	11.92	7.95	14.05	9.22	11.56	0.84
Average	2.38	2.22	12.17	8.10	14.38	9.42	11.56	0.82
BGF#1	6.05	4.42	21.95	13.98	28.51	17.90	20.18	0.89
BGF#2	6.07	4.44	22.51	14.30	32.24	21.34	20.18	1.06
BGF#3	7.05	5.02	20.25	12.94	27.58	17.34	20.18	0.86
Average	6.39	4.63	21.58	13.74	30.11	18.86	20.18	0.93

On BG specimens (repaired by grouting concrete), the average load causing initial cracking occurred when the load reached 2.38 kN, or M_{cr} equal to 2.22 kNm. The tensile reinforcement reached the yield stress when the load reached 12.17 kN, or M_y equal to 8.10 kNm. The ultimate beam capacity was achieved when the load reached 14.38 kN, or M_u equal to 9.42 kNm. It should be noted here that the estimated moment capacity of the test beam ($M_{u\text{-}est}$) was 11.56 kN. The ultimate moment capacity M_u of the beam was relatively lower than the estimated ultimate moment ($M_{u\text{-}est}$) with a ratio of 0.82. This was caused by premature damage to the interface between the existing concrete and the grouted concrete in the form of horizontal cracks. This horizontal crack indicated that the interface bond capacity was relatively smaller than the shear bond stress that occurred at the interface. Interface damage caused a decrease in the ultimate flexural capacity.

On BGF specimens (repaired by grouting concrete combined with FRP strengthening), the average load causing initial cracking occurred when the load reached 6.39 kN, or M_{cr} equal to 4.63 kNm. The tensile reinforcement reached the yield stress when the load reached 21.58 kN, or M_y equal to 13.74 kNm. The ultimate beam capacity was achieved when the load reached 30.11 kN, or M_u equal to 18.86 kNm. It should be noted here that the estimated moment capacity of the test beam ($M_{u\text{-}est}$) was 20.18 kN. The ultimate moment capacity M_u of the beam was relatively lower than the estimated ultimate moment ($M_{u\text{-}est}$) with a ratio of 0.93. Similar to the BG specimens, this was caused by premature damage to the interface between the existing concrete and the grouted concrete in the form of horizontal cracks. However, the interface failure occurred at a relatively higher load than the BG specimens due to the existing FRP strengthening. However, if the interface failure does not occur, then the beam capacity will be closer to the predicted value. The bonding interaction between the existing concrete and the grouting concrete also affected the strengthening effectiveness of FRP. The interaction between grouting and concrete was also affected by the surface treatment [9]. It

should be noted here that the surface treatment was only the removal of the cement dust and the application of a bonding agent before filling the concrete grout. The premature failure of bonding interaction due to shear stress caused the grouting layer to fail, and existing concrete was no longer in the form of composite interaction. Canaval et al. [13] have reported that an investigation of the reinforced concrete beams strengthened by wrapped grouting mortar with metallic connectors indicated shear failure.

Further observation, the BGF specimen showed that the flexural capacity of repaired beams (grooving and strengthening with GFRP) was still not significantly increased compared to the control specimen (BN). In estimating the flexural capacity of each type, it was designed that the specimens of BGF type had a flexural capacity of 35% above the control specimens. However, the flexural capacity between BGF and BN was relatively the same, or there was only a relatively small increase of 4%. Figure 9 shows the flexural capacity ratio compared to the BN-type specimens. Due to the longitudinal cracks that occurred on the interface between existing concrete and grouting concrete, the flexural action tended to behave as a non-bond. This may be illustrated in Figure 10. The failure of bonding interaction caused a decrease in the performance of the FRP sheet to strengthen the beam. The separation of the grouting layer and existing concrete, which was indicated by horizontal cracks, caused the FRP sheet to not fully interact with the compression concrete.

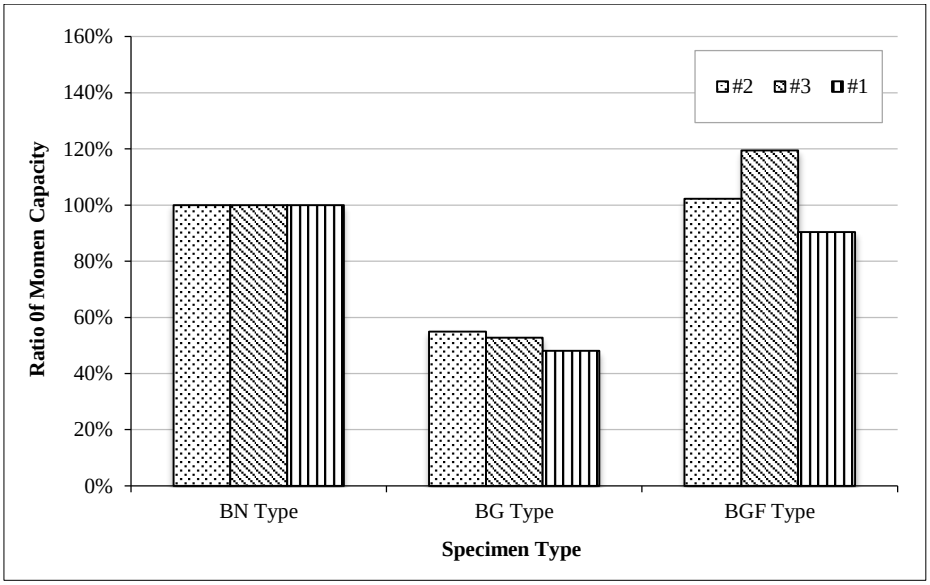

Figure 9. Ratio of Flexural Capacity Compared to Control Beam (BN)

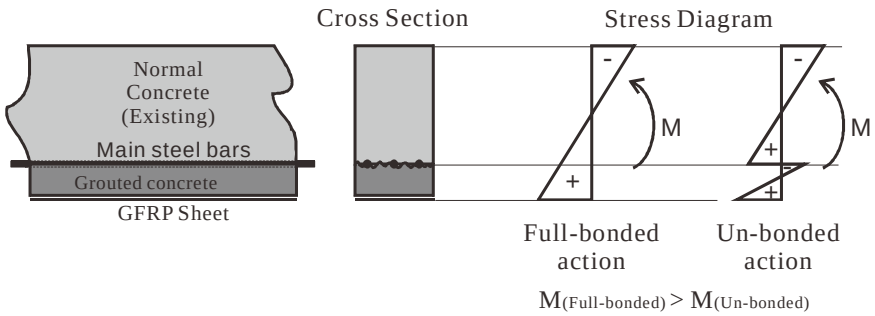

Figure 10. Full-bonded and Un-Bonded Flexural Action

The maximum flexural capacity may be achieved if grouted concrete and existing concrete have perfect bonding between each other, as illustrated in Figure 10. In the un-bonded condition, the layers of grouted concrete move each other in the area of contact. The full bond could be developed if the contact surface has enough shear capacity to resist shear stress. The shear stress at the contact surface may be obtained as follows:

$$\tau = \frac{VS}{Ib} \quad (1)$$

where V is shear force, S is first moment of area of the grouted concrete, I is moment of inertia of the entire cross section and b is the width of beam cross section.

It should be noted here that Equation 1 applies to uncracked elastic beams and is only an approximation for cracked concrete beams. The ACI Code gives an alternative of calculating the horizontal shear stress, as follows:

$$v_u = \frac{V_u}{bd} \quad (2)$$

where V_u is the shear force acting on the cross section of the beam as obtained from a shear-force diagram for the beam, *b* is width of the beam cross section, *d* is effective depth of cross section.

3.2. Load-Deflection Relationship

Figure 11 shows the load and deflection relationship at the mid-span of beams. Typical of the behavior of reinforced concrete beams, cracks occurred at relatively low applied loads when the ultimate stress of concrete had been reached. On the BG beam, the initial cracks occurred earlier than in the BN and BGF specimens. This occurred because the steel strain in the BG beam was relatively higher than that in the BN and BGF beams. It should be noted that the cross-section of the reinforcement in BG type was smaller to simulate a reduction of the steel reinforcement cross-section due to corrosion. In the BGF beam, although it used the same cross section of tensile reinforcement as the BG type, this specimen was strengthened with GFRP sheet, which contributed to delaying the achievement of the rupture stress in the concrete. The occurrence of initial cracks in the beam caused a decrease in beam stiffness. The BN beam experienced a change in initial stiffness from 3.88 kN/mm to 1.54 kN/mm. The BG beam experienced a change in initial stiffness from 1.77 kN/mm to 0.64 kN/mm, and the BGF beam experienced a change in initial stiffness from 4.65 kN/mm to 1.10 kN/mm. The biggest change in stiffness occurred in the BGF-type beam. This was due to the smaller GFRP modulus of elasticity (95 GPa) compared to steel reinforcement (200 GPa). After the steel strain reached the yield strain and entered the plastic phase, a change in the stiffness of the beam occurred again. The BN beam experienced a change in stiffness to 0.099 kN/mm.

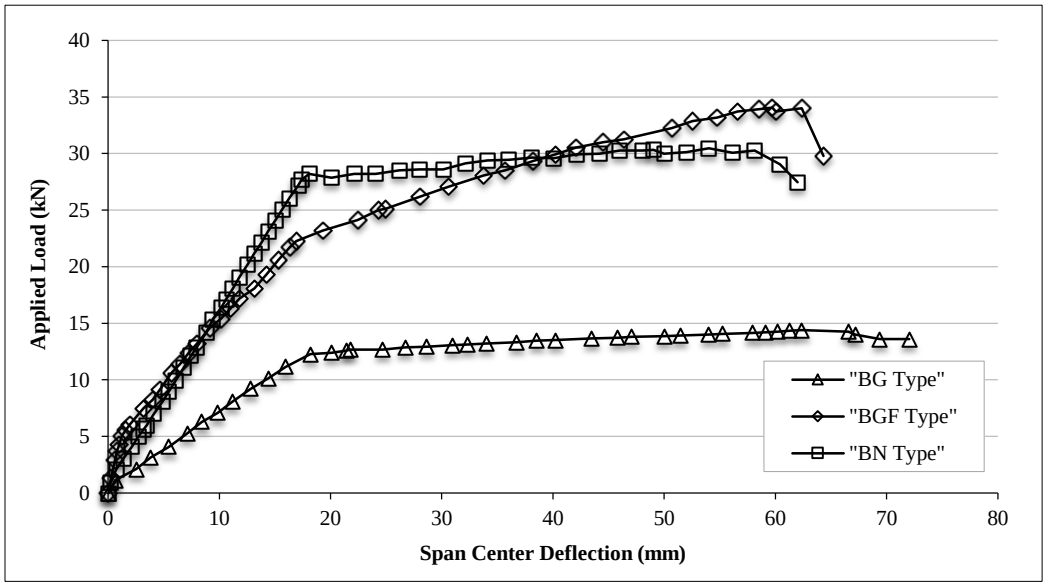

Figure 11. Load-Deflection Curve

The BG beam experienced a change in stiffness to 0.047 kN/mm, and the BGF beam experienced a change in stiffness to 0.282 kN/mm. As it can be observed, after the steel reinforcement was yielded, the change in stiffness of the BGF beam was relatively smaller compared to the other beams. This is because the BGF beam was still strengthened using the GFRP sheet.

3.3. Cracks Pattern and Failure Mode

Figure 12 shows the crack pattern of all specimens. In general, the first cracks occurred on the tension side of the beam (the bottom side of the beam) when the stress exceeded the concrete rupture strength. Cracks propagated from the tension side to the compression side as the applied load increased. For BN beams, the crack propagated to the compression section as on regular reinforced concrete beams. However, for BG and BGF beams, a layer of grouted concrete on the bottom side of the beam with a thickness of about 50mm showed a different crack pattern. At the beginning of loading, the vertical cracks appeared in a similar case with regular reinforced concrete beams. As the load increased, the vertical cracks continued to propagate, but they were also followed by the appearance of horizontal cracks. These horizontal cracks occurred at the interface between normal concrete and grouted concrete. The occurrence of horizontal cracks disrupted the bending interaction between the reinforcement on the tension side and the concrete on the compression side. This caused a reduction in the moment capacity. For BGF beams, a similar phenomenon also occurred. With the appearance of horizontal cracks, the GFRP sheets as reinforcement cannot interact effectively

anymore in resisting moments. This caused a decrease in momentary capacity. It can also be observed from Figure 12 that the repaired concrete beams (BG and BGF beams) had a smaller crack density in the span of the loading point (zero shear span) compared to the BN specimens. The crack density (number of cracks per unit length) of the BN type is 1.2 per meter. Meanwhile, the BG and BGF beams were 0.83 per meter and 0.65 per meter, respectively.

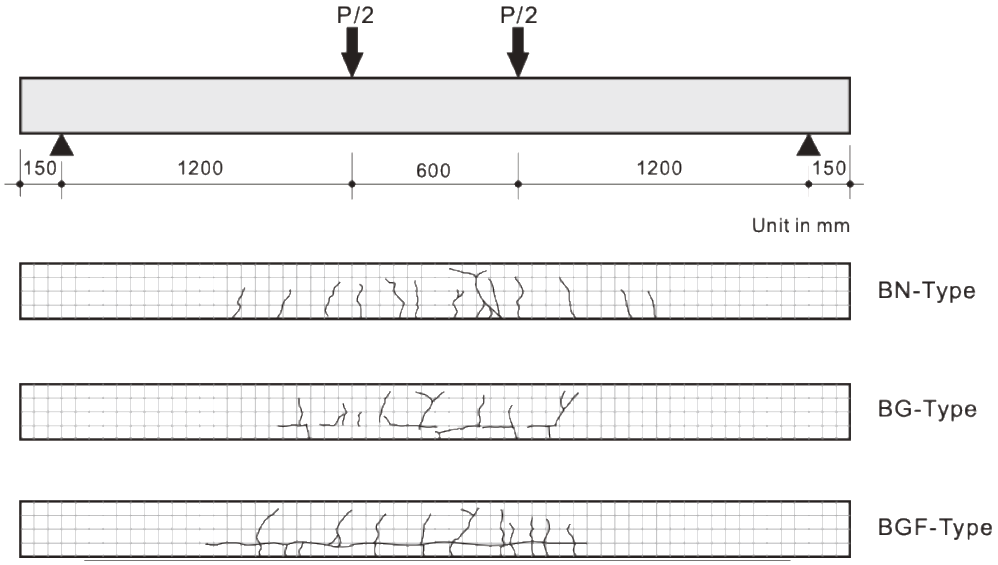

Figure 12. Crack Pattern of all beams

Figure 13 shows the modes of failure that occur on specimens. For the BN specimen, the mode of failure that occurred was similar to the general failure mode of regular reinforced concrete beams. The ultimate load was determined by the crushing of the concrete on the compression side after yielding the steel reinforcement on the tension side. Following the elongation of the tensile reinforcement due to the increased tensile force as an interaction with the compressive force, the number and length of cracks also increased. This mechanism continued until the concrete reached its crushing strength.

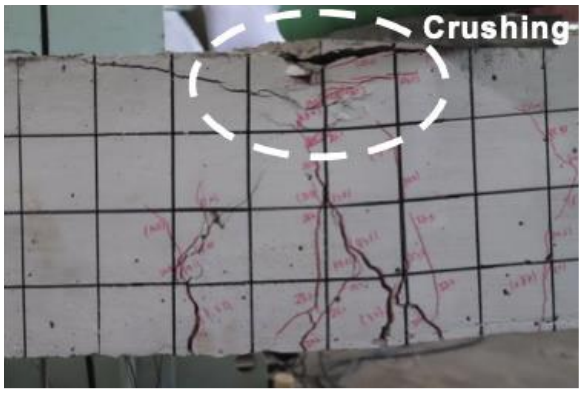

(a) Failure of BN Type

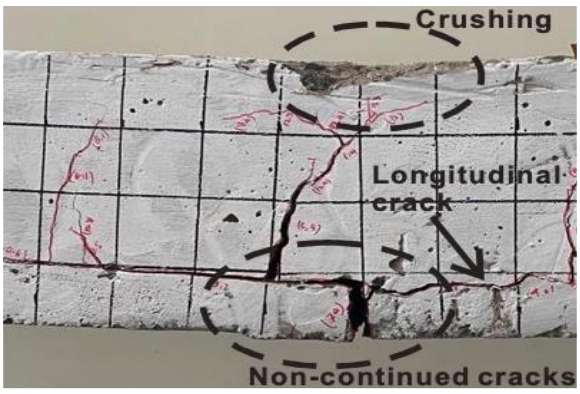

(b) Failure of BG Type

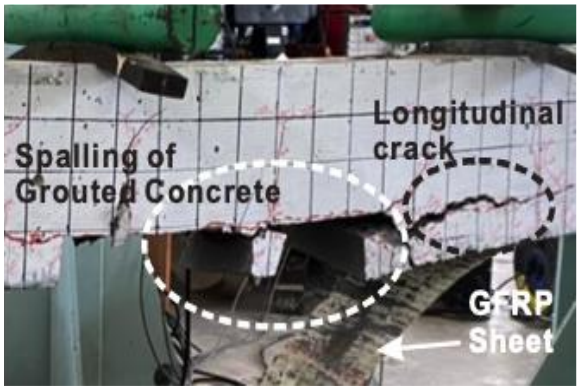

(c) Failure of BGF Type

Figure 13. Failure Mode of Beam Specimens

For BG and BGF type beams, a 50-mm grouted concrete layer on the tension side showed a different failure mechanism. For BG-type beams, cracks begin to occur in the grouted concrete when the stress exceeds the rupture stress of the grouted concrete. As the load increased, the cracks increased in both number and length. When the cracks reached the interface between grouted concrete and normal concrete, the horizontal cracks appeared. The appearance of longitudinal cracks indicates that the bonding stress or shear stress between the grouted concrete and the normal concrete was unable to maintain the monolith integration for longer. This caused the beam to tend to behave as a non-bonded sandwich beam. This phenomenon was indicated by the appearance of non-continued cracks in the beam, as may be observed in Figure 13.

The cracks propagated independently on grouted concrete and on normal concrete. The cracks in the normal concrete section moved towards the compression beam section. The BG beam reached its ultimate load when the concrete had reached its compressive strength. On BGF beams, crack propagation could be delayed due to the presence of GFRP sheet reinforcement on the bottom of the beams (the side of the grouted concrete surface). The GFRP sheet, together with steel reinforcement, resisted tensile forces due to the flexural action of the beam. After further loading, the bonding stress between the GFRP sheet and the grouted concrete surface reached its limit, and then debonding of the GFRP sheet occurred, followed by spalling of the grouted concrete. This caused a sudden decrease in the bending capacity of the beam.

4. Conclusion

Repairs of corroded steel-reinforced concrete beams using concrete grouting required strengthening using FRP sheets to restore the bending capacity of the beams. Strengthening the GFRP sheet on the simulated beams increased the flexural capacity close to that of the control beams. The failure mode on beams with grouting concrete was initiated with longitudinal cracks at the interface between existing concrete and the grouting concrete. This indicated that the interaction between the existing concrete and the grouting concrete was still relatively weak. The effectiveness of FRP sheet strengthening may be optimized when the occurrence of longitudinal cracks can be postponed or avoided. The premature failure of bonding interaction caused the grouting layer, and existing concrete was no longer in the form of composite interaction. The separation of the grouting layer and existing concrete, which was indicated by horizontal cracks, caused the FRP sheet to not fully interact with the compression concrete. Applying a special treatment to the surface and/or applying a mechanical anchor may be necessary to increase the bonding capacity of the grouting layer. However, this study has shown that the repairing method using concrete grouting on damaged concrete covers combined with strengthening using FRP sheets was an effective combination in repairing the corroded reinforced concrete beams.

5. Declarations

5.1. Author Contributions

Conceptualization, R.D. and R.I.; methodology, R.D.; validation, R.D., F., and K.Y.; formal analysis, R.D.; investigation, R.D.; resources, R.I.; data curation, R.D.; writing—original draft preparation, R.D.; writing—review and editing, F.; visualization, R.D.; supervision, K.Y.; funding acquisition, R.D. All authors have read and agreed to the published version of the manuscript.

5.2. Data Availability Statement

Data sharing is not applicable to this article.

5.3. Funding

The authors received no financial support for the research, authorship, and/or publication of this article.

5.4. Acknowledgements

A highly appreciation and gratitude to the Ministry of Education, Culture, Research and Technology of the Republic of Indonesia for funding this research through a Regular Fundamental Research scheme with contract number of 02381/UN4.22/PT.01.03/2023. Thank you is expressed also to the Structures and Materials Laboratory of Hasanuddin University and the students who have assisted in this research. Also, an appreciation to the Structure and Bridge Laboratory of Nagasaki University for advices.

5.5. Conflicts of Interest

The authors declare no conflict of interest.

6. References

[1] Mocová, K. A., Sackey, L. N. A., & Renkerová, P. (2019). Environmental Impact of Concrete and Concrete-Based Construction Waste Leachates. IOP Conference Series: Earth and Environmental Science, 290, 012023. doi:10.1088/1755-1315/290/1/012023.

[2] Huo, W., Zhu, Z., Chen, W., Zhang, J., Kang, Z., Pu, S., & Wan, Y. (2021). Effect of synthesis parameters on the development of unconfined compressive strength of recycled waste concrete powder-based geopolymers. Construction and Building Materials, 292. doi:10.1016/j.conbuildmat.2021.123264.

[3] Akhtar, A., & Sarmah, A. K. (2018). Construction and demolition waste generation and properties of recycled aggregate concrete: A global perspective. Journal of Cleaner Production, 186, 262–281. doi:10.1016/j.jclepro.2018.03.085.

[4] Fitriani, H., & Ajayi, S. (2023). Barriers to sustainable practices in the Indonesian construction industry. Journal of Environmental Planning and Management, 66(10), 2028–2050. doi:10.1080/09640568.2022.2057281.

[5] Goyal, A., Pouya, H. S., Ganjian, E., & Claisse, P. (2018). A Review of Corrosion and Protection of Steel in Concrete. Arabian Journal for Science and Engineering, 43(10), 5035–5055. doi:10.1007/s13369-018-3303-2.

[6] Sun, H., Zou, H., Li, X., Memon, S. A., Yuan, B., Xing, F., Zhang, X., & Ren, J. (2022). Combined Effects of Sulfate and Chloride Attack on Steel Reinforced Mortar under Drying–Immersion Cycles. Buildings, 12(8), 1252. doi:10.3390/buildings12081252.

[7] Zhang, X., Zhang, Y., Liu, B., Liu, B., Wu, W., & Yang, C. (2021). Corrosion-induced spalling of concrete cover and its effects on shear strength of RC beams. Engineering Failure Analysis, 127. doi:10.1016/j.engfailanal.2021.105538.

[8] Alwash, N. A., Kadhum, M. M., & Mahdi, A. M. (2019). Rehabilitation of corrosion-defected RC beam-column members using patch repair technique. Buildings, 9(5), 120. doi:10.3390/buildings9050120.

[9] Gergess, A. N., Shaikh Al Shabab, M., & Massouh, R. (2020). Repair of Severely Damaged Reinforced Concrete Beams with High-Strength Cementitious Grout. Transportation Research Record, 2674(6), 372–384. doi:10.1177/0361198120919116.

[10] Jung, J. S., Lee, B. Y., & Lee, K. S. (2019). Experimental Study on the Structural Performance Degradation of Corrosion-Damaged Reinforced Concrete Beams. Advances in Civil Engineering, 2019, 9562574. doi:10.1155/2019/9562574.

[11] Bin Jumaat, M. Z., Kabir, M., & Obaydullah, M. (2010). Structural performance of reinforced concrete beams repairing from spalling. European Journal of Scientific Research, 45(1), 89-102.

[12] Iskhakov, I., Ribakov, Y., Holschemacher, K., & Mueller, T. (2013). High performance repairing of reinforced concrete structures. Materials & Design, 44, 216-222. doi:10.1016/j.matdes.2012.07.041.

[13] Canaval, J. H., Silva, T. J. Da, & Santos, A. C. (2018). Experimental study of RC beams strengthened for bending by reinforced grout layer and connectors. Revista IBRACON de Estruturas e Materiais, 11(4), 810–833. doi:10.1590/s1983-41952018000400009.

[14] Peng, G., Niu, D., Hu, X., Zhong, S., & Huang, D. (2022). Experimental and theoretical study on the flexural behavior of RC beams strengthened with cementitious grout. Engineering Structures, 267, 114713. doi:10.1016/j.engstruct.2022.114713.

[15] Dangwal, S., & Singh, H. (2023). Seismic performance of corroded non-seismically and seismically detailed RC beam-column joints rehabilitated with High Strength Fiber Reinforced Concrete. Engineering Structures, 291, 116481. doi:10.1016/j.engstruct.2023.116481.

[16] Azam, R. (2016). Behaviour of Shear-Critical Reinforced Concrete Beams Strengthened with Fiber Reinforced Cementitious Mortar. PhD Thesis, University of Waterloo, Waterloo, Canada.

[17] Xie, F., Tian, W., Diez, P., Zlotnik, S., & Gonzalez, A. G. (2023). Bonding Performance of Glass Fiber-Reinforced Polymer Bars under the Influence of Deformation Characteristics. Polymers, 15(12), 2604. doi:10.3390/polym15122604.

[18] Yang, J., Haghani, R., Blanksvärd, T., & Lundgren, K. (2021). Experimental study of FRP-strengthened concrete beams with corroded reinforcement. Construction and Building Materials, 301. doi:10.1016/j.conbuildmat.2021.124076.

[19] Masoud, S., & Soudki, K. (2006). Evaluation of corrosion activity in FRP repaired RC beams. Cement and Concrete Composites, 28(10), 969–977. doi:10.1016/j.cemconcomp.2006.07.013.

[20] Al-Mashgari, H. A. Y., Hejazi, F., & Alkhateeb, M. Y. (2021). Retrofitting of corroded reinforced concrete beams in flexure using CFRP rods and anchor bolt. Structures, 29, 1819–1827. doi:10.1016/j.istruc.2020.12.047.

[21] Djamaluddin, R., Irmawaty, R., & Tata, A. (2016). Flexural capacity of reinforced concrete beams strengthened using GFRP sheet after fatigue loading for sustainable construction. Key Engineering Materials, 692, 66–73. doi:10.4028/www.scientific.net/KEM.692.66.

[22] Habeeb, M. N. (2022). Flexural behaviour of continuously supported FRP reinforced concrete beams. University of Bradford, Bradford, Iraq.

[23] Djamaluddin, R., & Irmawaty, R. (2017). Relationship Model of the Moment Capacity of GFRP Sheet Strengthened RC Beams to the Duration of Sea Water Exposure. Procedia Engineering, 180, 1195–1202. doi:10.1016/j.proeng.2017.04.280.

[24] Sultan, M. A., Djamaluddin, R., Tjaronge, W., & Parung, H. (2015). Flexural capacity of concrete beams strengthened using GFRP sheet after seawater immersion. Procedia Engineering, 125, 644–649. doi:10.1016/j.proeng.2015.11.092.

[25] Ali, H., Assih, J., & Li, A. (2021). Flexural capacity of continuous reinforced concrete beams strengthened or repaired by CFRP/GFRP sheets. International Journal of Adhesion and Adhesives, 104. doi:10.1016/j.ijadhadh.2020.102759.

[26] Kim, J., Jeong, S., Kim, H., Kim, Y., & Park, S. (2022). Bond Strength Properties of GFRP and CFRP according to Concrete Strength. Applied Sciences (Switzerland), 12(20), 10611. doi:10.3390/app122010611.

[27] Do-Dai, T., Chu-Van, T., Tran, D. T., Nassif, A. Y., & Nguyen-Minh, L. (2022). Efficacy of CFRP/BFRP laminates in flexurally strengthening of concrete beams with corroded reinforcement. Journal of Building Engineering, 53. doi:10.1016/j.jobe.2022.104606.